Two-dimensional ytterbium oxide nanodisks based biosensor for selective detection of urea

Ahmed A. Ibrahim, Rafiq Ahmad, Ahmad Umar, M.S. Al-Assiri, A.E. Al-Salami, Rajesh Kumar, S.G. Ansari, S. Baskoutas

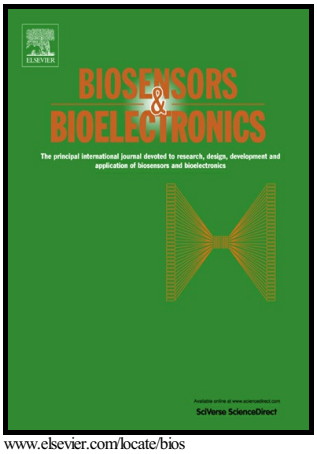

www.elsevier.com/locate/bios

PII: S0956-5663(17)30390-1
DOI: http://dx.doi.org/10.1016/j.bios.2017.06.015
Reference: BIOS9785

To appear in: *Biosensors and Bioelectronic*

Received date: 7 February 2017
Revised date: 6 June 2017
Accepted date: 8 June 2017

Cite this article as: Ahmed A. Ibrahim, Rafiq Ahmad, Ahmad Umar, M.S. Al-Assiri, A.E. Al-Salami, Rajesh Kumar, S.G. Ansari and S. Baskoutas, Two-dimensional ytterbium oxide nanodisks based biosensor for selective detection o urea, *Biosensors and Bioelectronic,* http://dx.doi.org/10.1016/j.bios.2017.06.015

Two-dimensional ytterbium oxide nanodisks based biosensor for selective detection of urea

Ahmed A. Ibrahim[a,b,c,1], Rafiq Ahmad[d,1], Ahmad Umar[a,b,1,*], M. S. Al-Assiri[b,e], A. E. Al-Salami[f], Rajesh Kumar[g], S.G. Ansari[h], S. Baskoutas[c]

[a]Department of Chemistry, Faculty of Science and Arts, Najran University, P.O. Box 1988, Najran-11001, Kingdom of Saudi Arabia

[b]Promising Centre for Sensors and Electronic Devices (PCSED), Najran University, P.O.Box-1988, Najran-11001, Kingdom of Saudi Arabia,

[c]Department of Materials Science, University of Patras, Patras GR-26504, Greece

[d]School of Semiconductor and Chemical Engineering, Nanomaterials Processing Research Center, Chonbuk National University, 567 Baekjedaero, Deokjin-gu, Jeonju-si, Jeollabuk-do, 54896, Republic of Korea.

[e]Department of Physics, Faculty of Science and Arts, Najran University, P.O. Box 1988, Najran-11001, Kingdom of Saudi Arabia

[f]Department of Physics, Faculty of Science, King Khalid University, P.O.Box-9004 Abha-61413, Kingdom of Saudi Arabia

[g]PG Department of Chemistry, JCDAV College, Dasuya-144205, Punjab, India.

[h]Centre for Interdisciplinary Research in Basic Sciences, Jamia Millia Islamia, New Delhi 110025, India.

*Corresponding Author. ahmadumar786@gmail.com

Abstract

Herein, we demonstrate synthesis and application of two-dimensional (2D) rectangular ytterbium oxide (Yb_2O_3) nanodisks via a facile hydrothermal method. The structural, morphological, compositional, crystallinity, and phase properties of as-synthesized nanodisks were carried out using several analytical techniques that showed Well defined 2D rectangular nanodisks/sheet like morphologies. The average thickness and edge length of the nanosheet structures were 20±5 nm and 600±50 nm, respectively. To develop urea biosensor, glassy carbon electrodes (GCE) were modified with Yb_2O_3

[1] **Authors contributed equally to this work.**

nanodisks, followed by urease immobilization and Nafion membrane covering (GCE/Yb_2O_3/Urease/Nafion). The fabricated biosensor showed sensitivity of 124.84 $\mu AmM^{-1}cm^{-2}$, wide linear range of 0.05-19 mM, detection limit down to ~2 μM, and fast response time of ~3s. The developed biosensor was also used for the urea detection in water samples through spike-recovery experiments, which illustrates satisfactory recoveries. In addition, the obtained desirable selectivity towards specific interfering species, long-term stability, reproducibility, and repeatability further confirms the potency of as-fabricated urea biosensor.

Keywords: Ytterbium oxide nanodisks; urease; urea biosensor

1. Introduction

Urea has been extensively used in agriculture as fertilizers, as de-icing agent, as stabilizers in soap and detergents (Cornell et al., 1998). However, their long-term usages will are not only increasing urea concentration in land and water but also they also can lead to soil acidification and eutrophication, which disturb the eco-system, cause death of aquatic life, and acute poisoning of cattle (Glibert et al., 2006; Anderson et al., 2002). Urea is a by-product of humans and mammals, and as an end product of nitrogen metabolism, urea levels in urine can determine liver and kidney issues (Coll et al., 2000). Normal urea level in the human blood is in the range of 2.5-7.5 mM, while abnormal levels (increased or decreased) in the blood causes serious diseases i.e. renal failure (acute or chronic), hepatic failure, gastrointestinal bleeding, dehydration, and nephritic syndrome (Bellomo et al., 2012; Clemmesen et al., 2001). Therefore, it becomes necessary to monitor the urea levels in physiological fluids (urine and blood) and in different domains including agriculture, food, pharmaceutical etc.

Yet, different analytical methods (i.e. gas chromatography, flourometric, calorimetry and chemiluminescence) have been studied for urea determination but these methods are expensive, time consuming, and not suitable for field-testing (Francis et al., 2002; Ayanoa et al., 2004; Hu et al., 1994; Dhawan et al., 2009). Recently, electrochemical based methods (i.e. amperometric and potentiometric) have attracted

great interest because of its remarkable advantages such as low fabrication cost, small size, high sensitivity and selectivity, low detection limit, and have potential ability for real-time and on-site analysis (Dhawan et al., 2009; Bo et al., 2017; Hahn et al., 2012; Bollella et al., 2017). However, to fabricate high performance electrochemical based biosensing electrodes, novel and promising nanostructured materials are highly required. As designed nanostructured materials used in biosensors fabrication provide various important features (i.e. high surface area-to-volume ratio, rapid electron communication, and an excellent matrix for enzyme immobilization) for improved biosensor performances. Furthermore, specifically for urea biosensor fabrication selecting a novel nanomaterial for urease immobilization during urea biosensor fabrication will not only result in high urease immobilization but also enhance the sensing performance for urea detection.

Unique chemistry and properties of the lanthanides elements, like unquenched magnetic moments, high magnetic susceptibilities, variable oxidation states, electropositive nature, electronic relaxation time, partially filled semi-core 4f subshell, long excited state lifetimes (>1 μs), high dielectric constants, high resistivity, large band gap energies *etc* make these elements and their compounds suitable for many advanced applications (Gillen et al., 2013; Zhang et al., 2016; Paik et al., 2013). Various lanthanide oxides such as La_2O_3, Sm_2O_3, CeO_2, Eu_2O_3, Gd_2O_3, Yb_2O_3, Pr_2O_3 etc. have been extensively applied in fields like electronics (Gillen et al., 2013), bioimaging proves (Paik et al., 2013), magnetic (Wang et al., 2011), phosphors (Tiwari et al., 2015), logic and memory devices (Pavunny et al., 2014; Kwo et al., 2000), catalysis (Wang et al., 2011; Cwik et al., 2006; Umar et al., 2015), electrochemical sensors (Umar et al., 2015), gas sensors (Zhang et al., 2013), temperature sensors and optical display devices (Zhao et al., 2008; Dey and Rai, 2014), ceramics (Azimi et al., 2013), solar cells (Hansen et al., 2016; Liu et al., 2014) and many more.

Tuning the size from bulk to nanoscale, tremendously improves the properties of these rare earth metal oxide materials and hence widens their scope of applications (Panda et al. 2007; Gai et al., 2014). Various methods have been reported in literature for synthesizing nanosized lanthanide oxides. Panda *et al.* reported a microwave irradiation

(MWI) method for the synthesis of organically passivated uniform, single crystalline rare earth oxide (Ln_2O_3, Ln=Pr, Nd, Sm, Eu, Gd, Tb, Dy) nanorods, and square nanoplates (Panda et al. 2007). Si *et al.* synthesized highly dispersible and crystalline rare earth oxide nanopolyhedra, nanoplates, and nanodisks through the thermolysis of benzoylacetonate complexes of the corresponding rare earth metals in oleicacid/oleylamine solvents (Si et al., 2005). Acetylacetonate and acetate precursors have also been reported using oleic acid/oleylamine/1-octadecene medium for synthesis of single-crystalline and monodisperse cubic rare earth oxide nanoplates and nanodisks (Si et al., 2007; Wang et al., 2014).

Among various lanthanide oxide nanomaterials, the ytterbium oxide (Yb_2O_3) is considered as an important *C-type* cubic refractory sesquioxide due to its high dielectric constant (~15), band gap energy (>5 eV) and remarkable chemical and thermal stabilities (Pan and Huang, 2009). Methods like co-precipitation (Liu et al., 2014), electro-spinning (Henriques et al., 2015), sol-gel (Dong et al., 2001), hydrothermal (Qian et al., 2013), solution-doping technique (Paul et al., 2010) *etc.*, are reported in literature for the synthesis of Yb_2O_3 nanostructures. Mainly, two-dimensional (2D) nanostructures of Yb_2O_3 could provide enhanced physical and chemical properties, high surface-to-volume ratio and good biocompatibility. Therefore, considering high specific surface area of 2D Yb_2O_3 nanostructures, an enhance enzyme immobilization capacity and biosensing performance could be expected. However, their implementation for biosensors fabrication has not been studied in depth.

In this paper, two-dimensional (2D) rectangular Yb_2O_3 nanodisks were synthesized via a facile hydrothermal route to evaluate urea biosensing characteristics. To the best of our knowledge, this is the first report on application of Yb_2O_3 nanodisks for urea detection in the form of a biosensor. In this biosensing, Yb_2O_3 nanodisks were used as support for enzyme immobilization, being rectangular shaped they provide large surface-to-volume ratio for enzyme loading. During electrochemical measurements, it was found that the modified GCE with Yb_2O_3 nanodisks and immobilized with urease showed excellent electrochemical characteristic for detection of urea. Moreover, fabricated urea biosensors (GCE/Yb_2O_3/Urease/Nafion) showed better performance in

terms of high sensitivity, wide linear range, lower detection limit, and excellent selectivity as compared with reported sensors. Furthermore, the feasibility of the proposed biosensor was tested in the water samples through spike-recovery experiments.

2. Materials and methods

2.1. Materials

Ytterbium chloride (111) hexahydrate ($YbCl_3.6H_2O$), hexamethylenetetramine (HMTA, 99%), ammonium hydroxide (NH_4OH), Jack bean urease type III (EC 3.5.1.5 from *Canavalia ensiformis*), urea, uric acid (UA), ascorbic acid (AA), glucose (Glu, d-(+)-99.5%), dopamine (DA), lactic acid (LA), sodium phosphate monobasic anhydrous (NaH_2PO_4), sodium phosphate dibasic dihydrate ($Na_2HPO_4{\cdot}2H_2O$), and sodium chloride (NaCl) were purchased from Sigma-Aldrich and used without further purification. Prior to the experiments, phosphate buffer saline solution (PBS; 50 mM, pH 7) was freshly prepared by mixing solutions of NaH_2PO_4, $Na_2HPO_4{\cdot}2H_2O$, and NaCl (0.9%) in deionized water. The enzyme solution was prepared in PBS solution after dissolving 1 mg/mL urease.

2.2. Synthesis of Yb_2O_3 nanodisks and characterizations

Two-dimensional (2D) rectangular Yb_2O_3 nanodisks were synthesized by a facile hydrothermal method. In a simple procedure, 0.01 M of each $YbCl_3.6H_2O$ and HMTA added in a beaker containing 50 mL of deionized water. The mixture solution was stirred for 30 min before adding few drops of NH_4OH to adjust the solution pH 6.4 and again stirred for 45 min. The resultant solution was subsequently transferred into Teflon-lined stainless steel autoclave and heated at 150 °C for 6h. After completion of reaction, the obtained product was washed with deionized water and ethanol many times and dried for overnight at room temperature. The dried sample was further annealed in air at 300 °C for 3 h.

The structure and morphology of the as-synthesized material was characterized by field emission scanning electron microscopy (FESEM; JEOL-JSM-7600F) and transmission electron microscopy (TEM, JEOL-JEM-2010) equipped with selected area

electron diffraction (SAED). The crystallinity and crystal phases of the synthesized materials were examined by X-ray diffraction (XRD; PAN analytical Xpert Pro.), measured with Cu-Kα radiation (λ = 1.54178 Å) in the range of 10-80° with a scan speed of 8° min^{-1}. The information about functional bonds was obtained by acquiring FTIR spectra using Perkin Elmer's FTIR spectrometer.

2.3. Fabrication of Yb_2O_3 nanodisks based urea biosensor and measurements

To fabricate urea-sensing electrode, first, the solution of as-synthesized Yb_2O_3 nanodisks was prepared after mixing Yb_2O_3 nanodisks and organic binder (butyl carbitol acetate) in 6:4 ratio under sonication. Then, 10 μL of dispersed solution was drop casted on the pre-cleaned GCE, followed by drying at room temperature. In the next step, 5μL of urease solution was dropped on the Yb_2O_3 nanodisks/GCE surfaces to immobilize urease by physical adsorption and dried at room temperature. Finally, 2μL Nafion solution was used to cover the modified electrode, which helps to protect electrode surface and reduce effect of interfering species on biosensor response. The electrode system has been termed as GCE/Yb_2O_3/Urease/Nafion.

All electrochemical measurements were carried out using an electrochemical measurement station (Ivium Compact State; Ivium Technologies) connected to computer with a modified (GCE/Yb_2O_3/Urease/Nafion) electrode as the working electrode, an Ag/AgCl (saturated KCl) reference electrode and a platinum (Pt) wire as counter electrode. The cyclic voltammetry (CV) and amperemetry (current *versus* time) were measured in 50 mM PBS (pH 7) in the potential range of -0.30 to +0.60V and at fixed voltage of +0.45V, respectively. The potentiostatic electrochemical impedance spectroscopy (EIS) measurements of the different modified electrodes were performed in 5 mM $K_3[Fe(CN)_6]$ redox probe (1:1 molar ratio) containing 100 mM KCl at an applied bias potential of 0.17 V and 5 mV amplitude within the frequency range from 0.1 Hz to 100 MHz.

3. Results and discussion

3.1. Morphological, structural, optical and compositional properties of Yb_2O_3 nanodisks

The morphologies of the as-synthesized Yb_2O_3 product were analyzed by FESEM technique. Low and high magnification FESEM images for as synthesized Yb_2O_3 are shown in Fig. 1 (a) and Fig. 1 (b), respectively. Well-defined Yb_2O_3 nanostructures having 2D rectangular nanodisks like morphologies with sharp corners and very smooth and flattened surfaces along with some nanosized particles can be clearly seen in the panoramic view (Fig.1 (b)). The average thickness and edge length of the nanosheet structures were 20 ± 5 nm and 600 ± 50 nm, respectively. Small sized aggregated Yb_2O_3 nanoparticles were also found on the surfaces of the nanodisks.

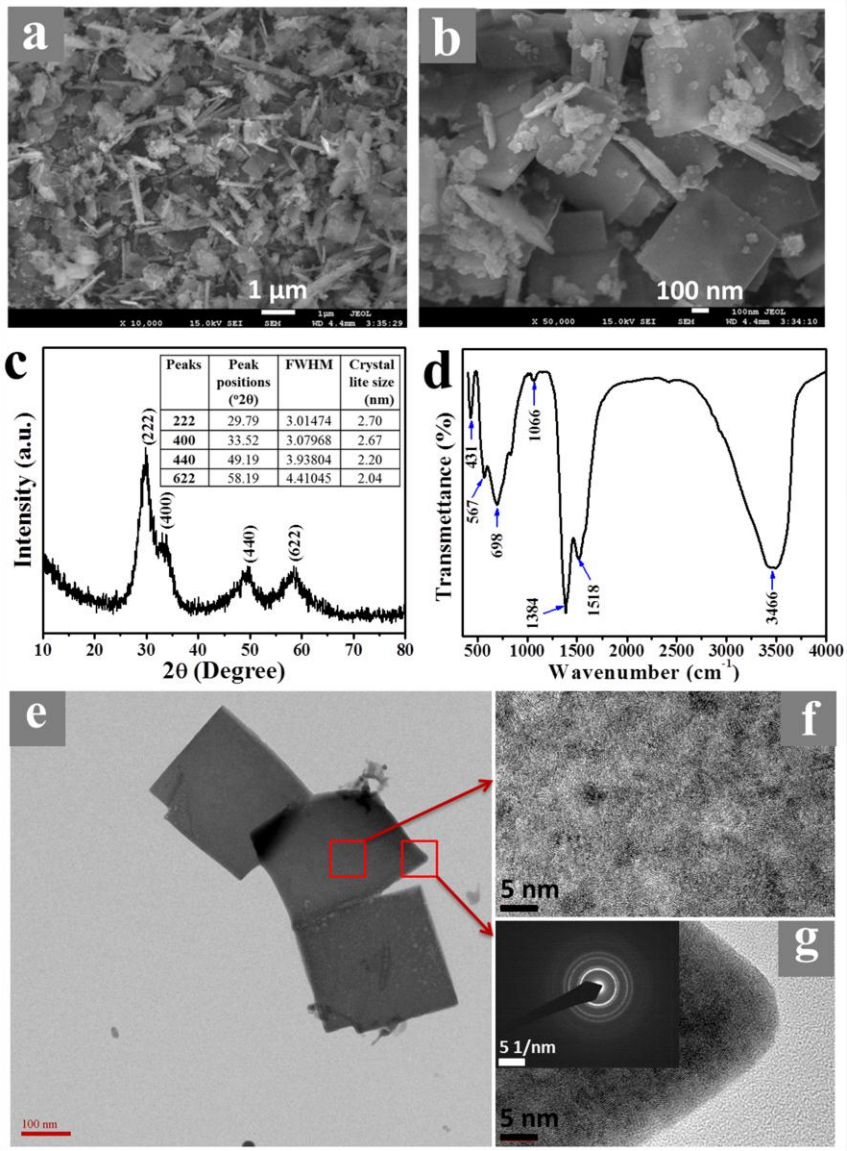

Fig. 1. (a) Low and (b) high magnification FESEM images; (c) XRD pattern and (d) FTIR spectrum; (e-g) low resolution and high-resolution TEM images of the as-synthesized 2D Yb_2O_3 rectangular shaped nanodisks. Inset (c) and (g) show the XRD data of Yb_2O_3 rectangular shaped nanodisks and SAED pattern, respectively.

Crystallographic and phase properties of the Yb_2O_3 powder were studied by XRD technique and shown in Fig. 1c. The diffraction peaks at 29.79^o, 33.52^o, 49.19^o, 58.19^o corresponding to the (222), (400), (440), (622) diffraction planes, respectively, are the characteristic peaks of the cubic phase of the Yb_2O_3. These peaks also match well with the JCPDS: 87-2374 for standard cubic phase of Yb_2O_3 as well as the reported literature

(Henriques et al., 2015; Bhattacharya et al., 2007; Pan et al., 2009). Broad peaks indicate that the particles are of nanosize.

Debye-Scherrer equation was used for the estimation of crystallite size (d) (Eq.1) (Patterson, 1939; Cullity and Stock, 2001).

$$d = \frac{0.89\,\lambda}{\beta \cos\theta} \quad \ldots\ldots\ldots\ldots (1)$$

Where, λ= the X-ray wavelength and is 1.54 Å, θ is the Bragg diffraction angle and β = full width at half maximum (FWHM). Each diffraction peak was explored to calculate FWHM and the crystallite size. The corresponding results are represented in the inset of Fig. 1c. The average crystallite size for 2D Yb_2O_3 rectangular shaped nanodisks was found to be 2.403 nm.

Fig. 1d represents FTIR spectrum for the Yb_2O_3 rectangular shaped nanodisks. Low intensity fingerprint region peaks at 431, 567, and 698 cm^{-1} can be assigned to the stretching vibrational modes of M-O (Yb-O) bonds (Nyquist and Kagel, 1971; Nakamoto, 1970). The absorption peaks at 1384 cm^{-1} may be due to the adsorbed CO_2 on the surface of Yb_2O_3 nanodisks during sample preparation (Kim et al., 2015; Nezamzadeh-Ejhieh and Zabihi-Mobarakeh, 2014). A broad band at 3466 $^{-1}$ can be seen due to the stretching vibrational modes of O-H groups of the adsorbed H_2O molecules (Umar et al., 2015; Umar et al., 2015).

The crystallinity of Yb_2O_3 rectangular shaped nanodisks were further confirmed using TEM and HRTEM and shown as Fig. 1e and 1f. The TEM images reveal the dimensions and crystal nature of as-synthesized Yb_2O_3 rectangular shaped nanodisks. The SAED pattern (inset of Fig. 1g), clearly shows the bright spots with rings, indicating high crystallinity. As shown in Fig 1g, the high resolution TEM exhibit well-defined lattice fringes without any visible disorder or dislocation in the lattices, which further confirmed that the synthesized nanodisks are well-crystalline without any impurity in the lattices.

3.2. Electrochemical behavior of the modified electrodes and urea biosensing performances

The overall schematic illustration of Yb_2O_3 nanodisks synthesis, GCE modification and its application for urea detection is depicted in Fig. 2a. The electrode characteristics were monitored using EIS to observe the impedance changes of the electrode surface during modification (Liu et al., 2017). Fig. 2b shows the Nyquist plots of bare GCE (i), Yb_2O_3/GCE (ii), and GCE/ Yb2O3/Urease/Nafion (iii) measured in 5 mM $K_3[Fe(CN)_6]$ redox probe (1:1 molar ratio) with 100 mM KCl supporting electrolyte at an applied bias voltage of 0.17V. The impedance data was obtained through the Randles equivalent circuit (inset of Fig. 2b), which shows a semicircular portion at high frequencies and a linear portion at low frequencies corresponding to the electron-transfer limited process and diffusion limited process, respectively. Meanwhile, the semicircle diameter at higher frequencies belongs to the electron-transfer kinetics of the redox probe at the electrode/electrolyte interface (Kang et al., 2017). From the Nyquist plots (Fig. 2b), the semicircular diameter (R_{ct}) of Yb_2O_3 modified GCE was much less (160 Ω, curve ii) than bare GCE (2704 Ω, curve i) and GCE/Yb_2O_3/Urease/Nafion (4216 Ω, curve iii). This suggests that the Yb_2O_3 modification improves the conductivity. However, after urease immobilization the R_{ct} value was enhanced due to hindrance caused by high enzyme adsorption over Yb_2O_3 nanodisks modified GCE, which further indicate the successful electrode fabrication. Additionally, the CV responses of electrodes were measured, shown in Fig. 2c. A well-defined redox peaks can be observed for GCE and Yb_2O_3 nanodisks modified GCE with the peak-peak separation of 491 and 133 mV, respectively. The decrease in peak-to-peak separation can be attributed to the Yb_2O_3 nanodisks modification, which provides high catalytic active surface area. However, almost no peaks were observed after urease immobilization and Nafion covering. The enzyme immobilization over nanostructures active area forms a blocking layer for $[Fe(CN)_6]^{3-/4-}$ to the electrode surface (Shrestha et al., 2017). As a result, significantly decrease current response was obtained for Nafion/urease/Yb_2O_3 modified electrode.

Fig. 2d displays the typical CV sweep curves of bare GCE (curves i and ii), GCE/Yb_2O_3/Urease/Nafion (curves iii and iv), GCE/Yb_2O_3/Nafion (curves v and vi), and GCE/Urease/Nafion (curves vii and viii) electrodes were recorded in 50 mM PBS (pH 7)

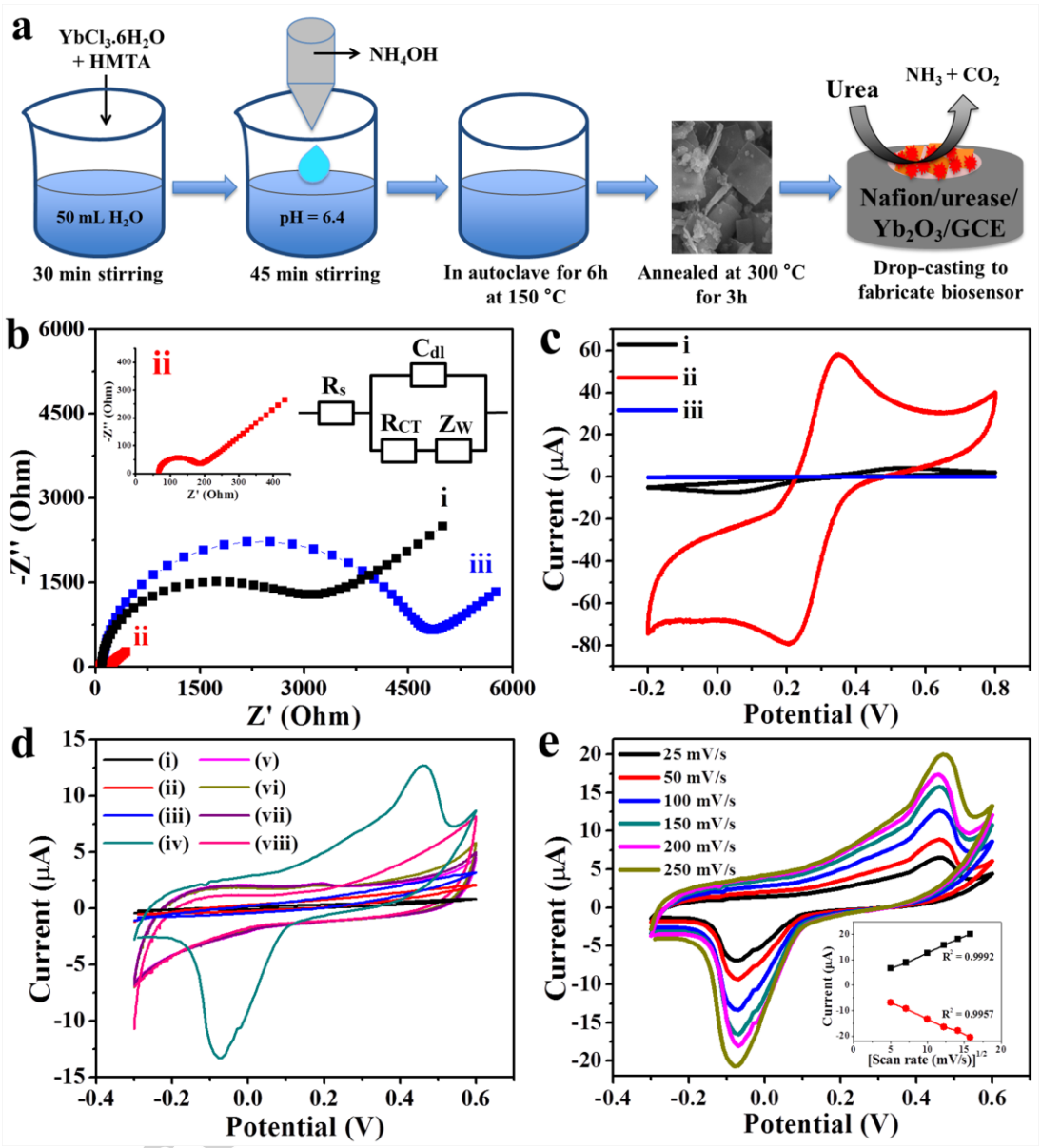

Fig. 2 (a) Schematic illustration of Yb_2O_3 nanodisks synthesis, GCE modification and its application for urea detection, (b) Nyquist plots and CV responses (c) of bare GCE (i), GCE/Yb_2O_3 (ii), and GCE/Yb_2O_3/Urease/Nafion (iii) in 5 mM $K_3[Fe(CN)_6]$ with 100 mM KCl supporting electrolyte, (d) Typical CV of the bare GCE (curves i and ii), GCE/ Yb_2O_3/Urease/Nafion (curves iii and iv), GCE/Yb_2O_3/Nafion (curves v and vi), and GCE/Urease/Nafion (curves vii and viii) electrodes in the absence (curves i, iii, v, and vi) and presence (curves ii, iv, vi, and viii) of 1 mM of urea in 50 mM PBS (pH 7) at a scan rate of 100 mV/s, and (e) CV sweep curves at different scan rates (25-250 mV/s) in the presence of 1 mM of urea. Inset b shows the magnified view of GCE/Yb_2O_3 Nyquist plot and Randles equivalent circuit and inset e shows plots of the anodic and cathodic peak current versus the square root of scan rates.

solution in the absence (curves i, iii, v, and vi) and presence (curves ii, iv, vi, and viii) of 1 mM of urea at 100 mV/s scan rate. In the absence of urea, bare GCE, GCE/Yb_2O_3/Nafion, GCE/Urease/Nafion, and GCE/Yb_2O_3/Urease/Nafion electrodes showed no peaks. However, in the presence of 1mM of urea only GCE/Yb_2O_3/Urease/Nafion electrode showed well-defined anodic and cathodic peaks at +0.45V and -0.08V, respectively. The appearance of peaks after urease immobilization is a clear indication of enzyme catalytic reaction, which catalyzes via hydrolysis of urea to carbamine acid that further gets hydrolyzed to ammonia (NH_3) and carbon dioxide (CO_2) in accordance with the following equation (Srivastava et al., 2013; Ahmad et al., 2015):

$$H_2N - CO - NH_2 + H_2O \xrightarrow{\text{Urease}} 2NH_3 + CO_2 \quad \text{.....(2)}$$

During the enzyme catalysis, the electrons generated are transferred to the GCE electrode that amplifies the electrochemical signal resulting in rapid biosensor response. The linear variation of the anodic and cathodic peak current increases with increasing scan rates from 25 to 250 mV/s (Fig. 2e). A linear variation of current as a function of square-root of scan rates (inset of Fig. 2e) indicates diffusion controlled electrochemical reaction is occurring on the electrode surface.

To evaluate the urea sensing performance of the fabricated biosensors (GCE/Yb_2O_3/Urease/Nafion), the amperometric response was measured with successive addition of different concentrations of urea from 0.05 to 25 mM, at a fixed potential of +0.45V in 50 mM PBS (pH 7). The obtained response is shown in Fig. 3a, wherein, the current increases linearly with increasing urea concentrations with slight non-linearity at higher urea concentrations i.e above 19 mM, probably due to the saturation/non-availability of enzymes active site (Fig. 3b). Also, from the above curve the detection limit and response time were estimated to be ~2 μM based on the signal and noise ratio of 3 (S/N = 3) and ~3s, respectively. The linear response of the biosensor to urea concentration ranging from 0.05 to 19 mM was obtained after performing three similar experiments. As shown in the Fig. 3b, the calibrated curve showed linear response with a correlation coefficient (R^2) of 0.9947. Further, the sensitivity of fabricated electrode was estimated to be 124.84 $\mu AmM^{-1}cm^{-2}$. The superior sensitivity of the developed urea biosensor as compared to reported data (listed in Table 1) could be due to the large

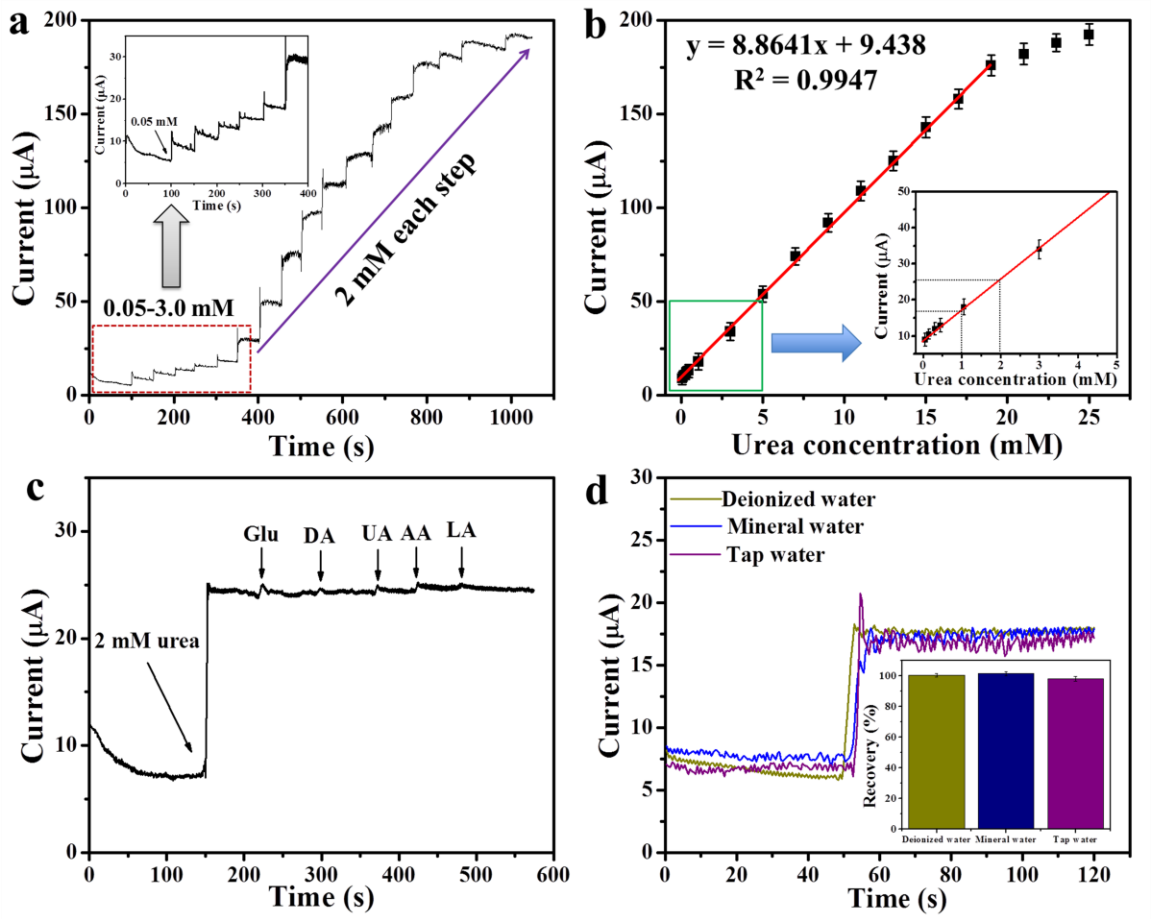

Fig. 3 (a) Amperometric response curve of GCE/Yb_2O_3/Urease/Nafion electrode with successive addition of in different concentrations (0.05 to 25 mM) of urea at a fixed applied potential of +0.45V in 50 mM PBS (pH 7), (b) calibration plot of urea concentration versus current response, (c) selectivity test to the subsequent addition of 2 mM of urea and 50 μM of each possible interfering agents i.e. Glu, DA, UA, AA, and LA in 50 mM PBS (pH 7) measured at a fixed applied potential of +0.45V, (d) amperometric response of GCE/Yb_2O_3/Urease/Nafion electrode in real sample analysis with 1 mM urea spiking at fixed applied potential of +0.45V. Insets a and d show the amperometric response to low concentration urea addition (0.05-3.0 mM) and histogram of real sample analysis using recover test, respectively.

surface-to-volume ratio of Yb_2O_3 rectangular shaped nanodisks, which provides higher surface area for enzyme loading. Especially, wide linear range and sensitivity are important parameters of biosensors that can significantly measure the low and high urea concentrations in real samples without any further dilution.

Table 1. Sensing performance comparison of urea biosensor based on Yb_2O_3 rectangular shaped nanodisks to previous reported data.

Electrodes	Sensitivity	Linear range (mM)	Detection limit (μM)	Response time (s)	Ref.
Urease/poly(glycidyl methacrylate-co-vinylferrocene/GCE	0.32 nA/mM	0.1-1.5	60	~3	(Çevik et al., 2012)
Urease/nanoporoussilicalite particles/Au	-	0.05-15	20	-	(Velychko et al., 2016)
Urease/ZnO-MWCNT/ITO	~43.02 μA $mM^{-1}cm^{-2}$	0.8-16.6	230	4	(Tak et al., 2013)
Urease/Chitosan-Fe_3O_4 composite/ITO	12.50 μA $mM^{-1}cm^{-2}$	0.8-16.6	330	10	(Kaushik et al., 2009)
Urease/ZnO-chitosan composite/ITO	0.13 μA $mM^{-1}cm^{-2}$	0.8-16.6	490	10	(Solanki et al., 2008)
Urease/ZrO_2 thin film/Au	0.07 μA $mM^{-1}cm^{-2}$	0.8-16.6	80	10	(Sumana et al., 2010)
GCE/Yb_2O_3/Urease/Nafion	**124.84 μA $mM^{-1}cm^{-2}$**	**0.05-19**	**~2**	**~3**	**This work**

3.3. Selectivity, long-term stability, reproducibility, and repeatability tests

The selectivity of GCE/Yb_2O_3/Urease/Nafion electrode was determined by measuring amperometric response at a fixed voltage of +0.45V in 50 mM PBS (pH 7). As shown in the Fig. 3c, after addition of 2 mM of urea the fabricated biosensor showed sensitive response for urea detection. However, the biosensor was nearly insensitive to the other interfering species i.e. Glu, DA, UA, AA, and LA. Hence, the good selective nature of urea biosensor electrodes can be attributed to the excellent enzyme-substrate affinity. Additionally, Nafion covering plays the dual role of facilitating electron transfer process from electrolyte to electrode surface and eliminate the interference effect of negatively charged interfering species such AA, UA and LA.

The long-term stability of as-fabricated urea biosensor (GCE/ Yb2O3/Urease/Nafion) was monitored using CV response curves in the presence of 1 mM of urea in 50 mM PBS (pH 7) for seven weeks. The urea biosensor retained 96.6% of its original oxidation peak current response, revealing good stability. Moreover, the reproducibility and repeatability were also evaluated by measuring CV response curves in the presence of 1 mM of urea in

50 mM PBS (pH 7) with similarly fabricated four bio-sensing electrodes and measuring CV response curves for up to 40 consecutive cycles, respectively. The relative standard deviation (RSD) of 3.8% for four sensors response and retain 97.4% of its initial current response after 40 consecutive cycles showed excellent reproducibility and repeatability, respectively. These results revealed excellent selectivity, good long-term stability, reproducibility and repeatability for urea detection.

3.4. Urea detection in real water samples (deionized, mineral and tap water)

In order to check the practical and analytical reliability of GCE/ Yb_2O_3/Urease/Nafion biosensors, deionized, mineral and tap water samples were used to measure 1 mM spiked urea using recovery test. Before spiking the known concentrations of urea (1 mM), the three buffer samples were prepared using all three water samples separately and their pH levels were maintained to 7. Then, the amperometric responses were measured at an applied potential of 0.45V, as shown in the Fig. 3d. The recovery percentage was calculated and is presented in inset of Fig. 3d, which showed best recovery in the deionized water sample. However, the recovery was satisfactory in the mineral and tap water samples. A slight decrease in the urea concentration recovery may be attributed to the presence of impurities and some common interfering agents. Furthermore, to compare the performance of the fabricated urea biosensor electrode with standard urea detection method, we used UV-Vis spectrophotometric-based method i.e.

Table 2. Comparison of the performance of our biosensor with the standard spectroscopic based method for the measurement of urea in real samples.

Sample	**Spiked urea**	**Urea concentrations**			
		Our method	Recovery (%)	Standard method (Spectroscopic method)	Recovery (%)
Deionized water	1 mM	100.4 ± 0.12	100.4	99.9 ± 0.08	99.9
Mineral water	1 mM	101.5 ± 0.14	101.5	100.2 ± 0.06	100.2
Tap water	1 mM	98.2 ± 1.24	98.2	99.4 ± 0.15	99.4

non-enzymatic p-dimethylaminobenzaldehyde (DMAB) method to measure urea concentration in deionized, mineral and tap water samples (Williams, 1984). Table 2 shows the performance comparison of our biosensor with the standard spectroscopic based method. From the obtained results, we could use these fabricated sensors in water samples and possibly extend the applications for urea detection in biological samples.

4. Conclusion

In summary, we have synthesized 2D rectangular Yb_2O_3 nanodisks via a facile hydrothermal route and employed for the first time to fabricate urea biosensor. The structural characterization results showed that the synthesized 2D rectangular Yb_2O_3 nanodisks were synthesized in large quantity and possess good crystallinity. The GCE electrodes modified with Yb_2O_3 nanodisks and immobilized urease exhibited excellent sensing performance i.e. high sensitivity (86.55 $\mu AmM^{-1}cm^{-2}$), wide linear range (0.05-20 mM), low detection limit (~2 μM), and fast response time (~3s), good selectivity, stability, reproducibility, and repeatability for the detection of urea. Overall, the obtained results showed superior electrochemical performance and Yb_2O_3 nanostructures might open a new sensing matrix to immobilize with desired enzyme and fabricate different sensing devices. Additionally, the developed biosensors could be used for urea detection in water samples.

Acknowledgements

The authors extend their appreciation to the Deanship of Scientific Research at King Khalid University for funding this work through research groups program under grant number R.G.P. 2/5/38.

References

Ahmad, R., Tripathy, N., Park, J.-H., Hahn, Y.-B., 2015. Chem. Commun. 51, 11968-11971.

Anderson, D., Glibert, P. M., Burkholder, J. M., 2002. Estuaries 25, 704-726.

Ayanoa, E., Kanazawab, H., Andoa, M., Nishimura, T., 2004. Anal. Chim. Acta 507, 211-218.

Azimi, G., Dhiman, R., Kwon, H.-M., Paxson, A. T., Varanasi, K. K., 2013. Nat. Mater. 12, 315-320.

Bellomo, R., Kellum, J. A., Ronco, C., 2012. The Lancet 380, 756-766.

Bhattacharya, A., Rao, R. S., Krishna, M. G., 2007. Sens. Actuators A Phy. 134, 348-356.

Bo, X., Zhou, M., Guo, L., 2017. Biosens. Bioelectron. 89, 167-186.

Bollella, P., Fusco, G., Tortolini, C., Sanzò, G., Favero, G., Gorton, L., Antiochia, R., 2017. Biosens. Bioelectron. 89, 152-166.

Çevik, E., Şenel, M., Abasıyanık, M. F., 2012. J. Solid State Electrochem. 16, 367-373.

Clemmesen, J. O., Kondrup, J., Nielsen, L. B., Larsen, F. S., Ott, P., 2001. Am. J. Gastroenterol. 96, 1217-1223.

Coll, E., Botey, A., Alvarez, L., Poch, E., Quintó, L., Saurina, A., Vera, M., Piera, C., Darnell, A., 2000. Am. J. Kidney Dis. 36, 29-34.

Cornell, S. E., Jickells, T. D., Thornton, C. A., 1998. Atmos. Environ. 32, 1903-1910.

Cullity, B. D., Stock, S. R., 2001. Elements of X-ray diffraction, 3rd edition, Prentice Hall.

Cwik, A., Hell, Z., Figueras, F., 2006. Adv. Synth. Catal. 348, 523-530.

Dey, R., Rai, V. K., 2014. Dalton Trans. 43, 111-118.

Dhawan, G., Sumana, G., Malhotra, B. D., 2009. Biochem. Eng. J. 44, 42-52.

Dong, X. T., Liu, G. X., Sun, J., Li, J. L., Liu, J. H., Hong, G. G., 2001. Rare Metal Mat. Eng. 30, 73-76.

Francis, P. S., Lewis, S. W., Lim, K. F., 2002. TrAC-Trends Anal. Chem. 21, 389-400.

Gai, S., Li, C., Yang, P., Lin, J., 2014. Chem. Rev. 114, 2343-2389.

Gillen, R., Clark, S. J., Robertson, J., 2013. Phys. Rev. B 87, 125116.

Glibert, P. M., Harrison, J., Heil, C., Seitzinger, S., 2006. Biogeochem. 77, 441-463.

Hahn, Y.-B., Ahmad, R., Tripathy, N., 2012. Chem. Commun. 48, 10369-10385.

Hansen, P., Fjellvåg, H., Finstad, T., Nilsen, O., 2016. J. Vac. Sci. Technol. A 34, 01A130.

Henriques, M. S., Ferreira, A. C., Cruz, A., Ferreira, L. M., Branco, J. B., Brázda, P., Jurek, K., Stora, T., Gonçalves, A. P., 2015. Ceram. Int. 41, 10795-10802.

Hu, X., Takenaka, N., Kitano, M., Bandow, H., Maeda, Y., Hattori, M., 1994. Analyst 119, 1829-1833.

Kang, Z., Jiao, K., Yu, C., Dong, J., Peng, R., Hu, Z., Jiao, S., 2017. RSC Adv. 7, 4572-4579.

Kaushik, A., Solanki, P. R., Ansari, A. A., Sumana, G., Ahmad, S., Malhotra, B. D., 2009. Sens. Actuators B 138, 572-580.

Kim, S. H., Umar, A., Kumar, R., Ibrahim, A. A., Kumar, G., 2015. Mater. Lett. 156, 138-141.

Kwo, J., Hong, M., Kortan, A. R., Queeney, K. T., Chabal, Y. J., Mannaerts, J. P., Boone, T., Krajewski, J. J., Sergent, A. M., Rosamilia, J. M., 2000. Appl. Phys. Lett. 77, 130.

Liu, T., Bai, X., Miao, C., Dai, Q., Xu, W., Yu, Y., Chen, Q., Song, H., 2014. J. Phys. Chem. C 118, 2908-2918.

Liu, Q., Ma, C., Liu, X.-P., Wei, Y.-P., Mao, C.-J., Zhu, J.-J., 2017. Biosens. Bioelectron. 92, 273-279.

Nakamoto, K. I., 1970. Spectra of Inorganic and Coordination Compounds, second ed., Wiley, Eastern NY.

Nezamzadeh-Ejhieh, A., Zabihi-Mobarakeh, H., 2014. J. Ind. Eng. Chem. 20, 1421-1431.

Nyquist, R. A., Kagel, R. O., 1971. Infrared Spectra of Inorganic Compounds, Academic Press, Inc, New York, London.

Pan, T. M., Chen, F. H., Lee, C. D., Chien, Y. K., Ko, H. M., 2009. Int. Semiconductor Device Research Symposium ISDRS 09.

Pan, T. M., Huang, W. S., 2009. Appl. Surf. Sci. 255, 4979-4982.

Panda, A. B., Glaspell, G., Samy El-Shall, M., 2007. J. Phys. Chem. C 111, 1861-1864.

Patterson, A. L., 1939. Phys. Rev. 56, 978-982.

Paul, M. C., Upadhyaya, B. N., Das, S., Dhar, A., Pal, M., Kher, S., Dasgupta, K., Bhadra, S. K., Sen, R., 2010. Opt. Commun. 283, 1039-1046.

Pavunny, S. P., Scott, J. F., Katiyar, R. S., 2014. Materials (Basel) 7, 2669-2696.

Qian, C., Zeng, T., Liu, H., 2013. Adv. Condens. Matter .Phys. 2103, 519869.

Si, R., Zhang, Y. W., You, L. P., Yan, C. H., 2005. Angew. Chemie . Int. Ed. 44, 3256-3260.

Si, R., Zhang, Y. W., Zhou, H. P., Sun, L. D., Yan, C. H., 2007. Chem. Mater. 19, 18-27.

Shrestha, B. K., Ahmad, R., Shrestha, S., Park, C. H., Kim, C. S., 2017. Biosens. Bioelectron. 94, 686-693.

Srivastava, S., Ali, M. A., Solanki, P. R., Chavhan, P. M., Pandey, M. K., Mulchandani, A., Srivastava, A., Malhotra, B. D., 2013. RSC Adv. 3, 228-235.

Sumana, G., Das, M., Srivastava, S., Malhotra, B. D., 2010. Thin Solid Films 519, 1187-1191.

Solanki, P. R., Kaushik, A., Ansari, A. A., Sumana, G., Malhotra, B. D., 2008. Appl. Phys. Lett. 93, 163903.

Tak, M., Gupta, V., Tomar, M., 2013. J. Mater. Chem. B 1, 6392-6401.

Tiwari, S., Singh, S., Kumar, K., Rai, V., 2015. Adv. Sci. Lett. 21, 2618-2620.

Umar, A., Kumar, R., Akhtar, M. S., Kumar, G., Kim, S. H., 2015. J. Colloid Interface Sci. 454, 61-68.

Umar, A., Kumar, R., Kumar, G., Algarni, H., Kim, S. H., 2015. J. Alloys Compd. 648, 46-52.

Velychko, T. P., Soldatkin, O. O., Melnyk, V. G., Marchenko, S. V., Kirdeciler, S. K., Akata, B., Soldatkin, A. P., El'skaya, A. V., Dzyadevych, S. V., 2016. Nanoscale Res. Lett. 11, 106-111.

Wang, G., Peng, Q., Li, Y., 2011. Acc. Chem. Res. 44, 322-332.

Wang, L., Ma, Y., Wang, Y., Liu, S., Deng, Y., 2011. Catal. Commun. 12, 1459-1462.

Williams S, 1984. Official Methods of Analysis of the Association of Official Analytical Chemists. Association of Official Analytical Chemists; Colombia, Maryland.

Zhang, G., Zhang, S., Yang, L., Zou, Z., Zeng, D., Xie, C., 2013. Sens. Actuators B Chem. 188, 137-146.

Zhang, X., Wang, Y., Cheng, F., Zheng, Z., Du, Y., 2016. Sci. Bull. 61, 1422-1434.

Zhao, X., Wang, X., Lin, H., Wang, Z., 2008. Phys. B Condens. Matter. 403, 1787-1792.

Highlights

- Synthesis of 2D rectangular ytterbium oxide (Yb_2O_3) nanodisks via a facile hydrothermal method.
- Rectangular shaped nanodisks provide large surface-to-volume ratio for urease enzyme loading.
- Fabricated biosensor showed high sensing performance during urea detection.
- The proposed biosensor was successfully employed for urea detection in real water samples.